K-Ar AND Rb-Sr DATING OF NANOMETER-SIZED SMECTITE-RICH MIXED LAYERS FROM BENTONITE BEDS OF THE CAMPOS BASIN (RIO DE JANEIRO STATE, BRAZIL)

Norbert Clauer[1]*, Jan Środoń[2], Amélie Aubert[3], I. Tonguç Uysal[4], and Theofilos Toulkeridis[5]

[1]Institut de Physique du Globe de Strasbourg, Université de Strasbourg (UdS-CNRS), 1 Rue Blessig, 67084 Strasbourg, France
[2]Institute of Geological Sciences, Polish Academy of Sciences, 31-002 Kraków, Poland
[3]Laboratoire d'Hydrologie et de Géochimie de Strasbourg, Université de Strasbourg (UdS-CNRS), 1 rue Blessig, 67084 Strasbourg, France
[4]Geological Engineering Department, Ankara University, Gölbaşı, Ankara, Turkey
[5]Universidad de las Fuerzas Armadas ESPE, Av. General Ruminahui, Sangolqui, Ecuador

Abstract—K-Ar isotopic dating has been applied to alkali-rich nanometer-sized illite separates of bentonites since the late 1990s. In the present study, K-Ar and Rb-Sr isotopic analyses were based on mineralogical determinations and morphological observations of similarly nm-sized separates (<0.02, 0.02–0.05, and 0.05–0.1 μm) depleted in alkalis and recovered from Santonian (85.8–83.5 Ma) bentonites of the Campos Basin located offshore the southeastern Atlantic coast (Rio de Janeiro State, Brazil). On the basis of XRD analyses and geochemical/mineralogical simulations, the size fractions consist essentially of the smectite-rich end-member of the smectite-to-illite trend with no more than 9% authigenic illite layers. High K-Ar values from 42.6 ± 3.2 to 70.2 ± 2.1 Ma confirm the occurrence of detrital illite in one sample at least, the age data being meaningless. A second group of K-Ar values ranges from 15.5 ± 10.7 to 41.3 ± 10.8 Ma, while the smallest (<0.02 and 0.02–0.05 μm) fractions with <0.42% K_2O lack detectable radiogenic ^{40}Ar and yield analytically 0 Ma ages. Two samples including that with the detrital illite were leached with dilute acid and the Rb-Sr method was applied to the untreated, leachate, and residual fractions of the different separates. The combined isotopic data suggest that illitization started at ~44 ± 4 Ma when the bentonites were subjected to a temperature of ~60°C. The leachable Sr yielded $^{87}Sr/^{86}Sr$ ratios of 0.7106–0.7108, which is greater than those of seawater either during deposition or recently, and of the initial ashes. They do not correspond to the chemical signature of pore fluids, but more likely to removals from fragile edges of the illite-smectite layers probably impacted by the rough initial chemical treatment applied to empty the smectite interlayers. Illitization was either a side effect of a major contemporaneous smectitization or an independent process that occurred later, in the progressively buried bentonite beds. Of variable duration, it was probably dependent on burial-induced temperature increase in the bentonites, which monitored the fixation of K in the smectite layering with or without a changing fluid chemistry. On the basis of the combined K-Ar and Rb-Sr isotopic data, illitization lasted either until ~15 Ma or even 0 Ma for some of the finest size fractions.

Keywords—Basin history · Bentonite beds · Campos Basin (Rio de Janeiro State · Brazil) · K-Ar and Rb-Sr isotopic dating · Scanning electron microscopy · Smectite and illite authigenesis · X-ray diffraction

INTRODUCTION

Since the pioneering isotopic studies on sized clay materials, the reliability of the ages obtained has been questioned because of a possible retention deficiency of the radiogenic isotopes. This controversy started in the late 1950s with glauconite separates often giving ages younger than the stratigraphic age of the host rocks (e.g. Hurley et al. 1960; Aronson and Hower 1976). Diagenetic crystallization of authigenic clay minerals younger than their host sediments raised the possibility of an alternative loss of radiogenic isotopes facilitated by the decrease in their particle size. For completeness, one should recall that data from some of these glauconites are also older than their stratigraphy, a fact that has seldom been emphasized because age records of minerals partly or completely of detrital origin are expected to be older than those of the host sediments. In fact, detrital mica-type crystals survive in sediments up to the anchizone/epizone boundary (e.g. Hunziker et al. 1986),

which explains such older ages in clay minerals up to burial diagenetic and anchi-metamorphic conditions. At the same time and in the same diagenetic zone, crystallization of new clay minerals such as mixed-layer illite-smectite and even illite explains ages younger than the stratigraphic records (Velde and Vasseur 1992; Renac and Meunier 1995; Altaner and Ylagan 1997).

The decrease in isotopic age with decreasing particle size in diagenetic clay material has been and still is generally interpreted as resulting from a decrease in the content of detrital contaminants (e.g. Perry 1974; Ehrenberg and Nadeau 1989; Pevear 1992; Środoń et al. 2002). A convincing analytical example for this interpretation was published by Reuter (1987) in a comparative study of low-grade metamorphic shales and associated tuffs from the Rhenish Massif (Germany). There, the shales outline a stepwise decreasing age when the grain size of the analyzed separates decreases, whereas the associated tuffs yield an age pattern that remains constant relative to grain size. This flat repartition of the ages was due precisely to the absence of detrital components in the volcanic material, whereas the staircase distribution of the same size

fractions in the associated shales resulted necessarily from the decreasing content of detrital minerals in the finer size fractions. As no radiogenic isotope loss could be detected, the author concluded that, if occurring at all in shales, it could certainly not be considered as a rule. On the other hand, Szczerba et al. (2015) performed a molecular modeling of the ^{40}Ar atom during natural radioactive decay of ^{40}K into ^{40}Ar. Those authors concluded that due to a high kinetic energy some ^{40}Ar atoms are potentially able to leave the interlayer position to embed nearby even in the opposite tetrahedral sheet of the neighboring silicate layers. Such atoms may then leave the illite particle over geological time, especially when located at the crystal edges. Thus, an age decrease should occur and be greatest for the thinnest crystals. The maximum age decrease due to such an effect was evaluated as 10%, but this hypothesis has not been verified experimentally so far.

Isotopic ages younger than the stratigraphy, due to a potential diffusion of radiogenic isotopes from clay materials, have also been studied experimentally at various temperatures and durations since the early 1970s (e.g. Thompson and Hower 1973; Odin et al. 1977; Odin and Bonhomme 1982; Zimmermann and Odin 1982; Clauer et al. 1984; Aronson and Douthitt 1986; Hunziker et al. 1986) with no clear evidence of radiogenic ^{40}Ar escape. Interestingly, an alternative trend of an age increase with a particle size decrease was also described from nanometer-sized diagenetic illite crystals of bentonites devoid of any detrital component (Clauer et al. 1997; Środoń et al. 2002; Środoń et al., 2009a, b). Such a trend was explained by the crystal-growth theory of Eberl et al. (1998), which predicted that coarser nm-sized clay crystals yield younger ages than their finer equivalents because they incorporate new material faster and, therefore, grow faster. In fact, any illite-type mineral may lose K during any diagenetic alteration, but independently of its particle size (e.g. Clauer 2011; Clauer and Mongodin 2012).

The ability of clay minerals, especially K-rich illite, to lock radiogenic isotopes in their crystal structures remains an important issue in isotopic dating of authigenic clay minerals from buried sediments. Burial as a very common natural process associated systematically with temperature increase, therefore, favors authigenesis of such clay minerals, but also induces a preferential diffusion of radiogenic ^{40}Ar relative to radiogenic ^{87}Sr, again only of clay components in thermic-chemical disequilibrium (Clauer et al. 1999; Lerman et al. 2007). As mentioned above, any thermal alteration of detrital clay materials of any size affects the retention potentials of their radiogenic isotopes, as does any type of alteration on any type of mineral.

In isotopic dating, the smectite to illite trend (labeled I-S hereafter) applies to all particles containing more or less K-tied layers, according to the kinetic model of a theoretical reaction path (Essene and Peacor 1995). Their K-Ar and Rb-Sr isotopic systems are then controlled by the progressive incorporation of alkalis into the interlayers, the course of illitization being routinely identified by XRD analysis since the mid-1950s

(e.g. Weaver 1957; Burst 1959; Powers 1959; Dunoyer de Segonzac 1970; Hower et al. 1976; Środoń and Eberl 1984; Velde 1985). The isotopic behavior of such I-S materials during illitization (Hower et al. 1976) was linked originally to the traditional smectite-to-illite transformation mechanism (Lee et al. 1989; Hamilton et al. 1989, 1992). At about the same period, this solid-state process was challenged with a model integrating the dissolution of smectite layers substituted simultaneously by the nucleation of illite layers (Inoue et al. 1987; Eberl and Środoń 1988; Pollastro 1993). Nadeau et al. (1984) were the first to separate, study, and identify such K-rich illite crystals resulting from crystallization and growth of illite layers in I-S structures, which they called "fundamental particles." Depending on the mechanism of illitization, solid-state transformation or dissolution/precipitation, and assuming that particle-size separation was completed successfully, one might expect different isotopic records for populations of illite crystals of varied sizes that depend on the type of host rock and the initial smectite, the duration of the process, and the chemistry of the interacting pore waters. Clauer et al. (2018) tried to decrypt some of these illitization processes by studying the isotope composition, contents, and location of B in illite layers by nuclear magnetic resonance analysis. By now, and depending on the intrinsic illitization process, the different isotopic trends obtained for nm-sized illite crystals, mostly of bentonites (e.g. Clauer et al. 1997; Honty et al. 2004), suggest varied processes for the smectite-to-illite trend. Since then, this methodology has been extended to illite particles from sandstones to evaluate time fluctuations of illitization in a sedimentary basin, and to develop some kinetic models (e.g. Środoń et al. 2002, 2006; Clauer et al. 2003, 2004).

The present study was conceived in this context to gain more information about the smectite-to-illite process by studying the smectite-rich end-member of the trend, with a challenging aspect for the K-Ar and Rb-Sr analytical procedures. Indeed, the expectations were about the analysis of smectite-rich I-S containing very small amounts of K and Rb at the onset of illitization and, therefore, measuring small to very small amounts of radiogenic ^{40}Ar and ^{87}Sr. The goal was to check if even a limited number of illite layers is able to store radioactive ^{40}K and ^{87}Rb, as well as radiogenic ^{40}Ar and ^{87}Sr within a crystalline structure characterized by its overall lack of interlayer sites where these isotopes are usually keyed. The samples analyzed were smectite-rich bentonite layers from the Campos Basin located offshore the State of Rio de Janeiro (Brazil). Because the bentonite lithology is generally lacking detrital minerals unless bioturbated with the hosting shales, this rock type was often selected for dating initial illitization after an early, low-T devitrification of the volcanic ash. This devitrification is often accompanied by a diagenetic precipitation of authigenic smectite-rich materials (Altaner et al. 1984; Elliott and Aronson 1987; Calarge et al. 2002). Of course, the challenge of analyzing crystals with very

small alkali contents depends also on how the analytical equipment used is able to handle very small amounts of radioactive ^{40}K and ^{87}Rb and radiogenic ^{40}Ar and ^{87}Sr; this was the key analytical challenge.

ANALYTICAL PROCEDURE

Reduced by hand to cm^3-sized rock chips, the bentonite samples were stored in polyethylene bottles filled with de-ionized water for disaggregation by freeze-thaw cycles (Liewig et al. [1987]). This method avoids any overgrinding and, therefore, any artificial reduction of large framework minerals into the size of the clay minerals. Then, the <2 μm fractions were recovered by sedimentation of the clay suspension in de-ionized water and the slurries were treated with sodium-acetate, sodium dithionite, and hydrogen peroxide to remove the soluble mineral phases, the organic matter, and the free cations adsorbed on and hosted within the mineral structures (Jackson, [1975]). Of course, these chemical products were ultra-pure to avoid any pollution of the I-S fractions during their interaction. Afterward, the <0.2 μm fractions were collected from <2 μm fractions by centrifugation and were diluted to a concentration of 1 g of powder in 40 L of de-ionized water to ensure "infinite" osmotic swelling (Środoń et al. [1992]). This further separation into the smallest micrometric and nanometer sizes (<0.02, 0.02–0.05, 0.05–0.1, and 0.1–0.2 μm) was completed by continuous, high-speed flow in an ultra-centrifuge coupled with a flow meter. The nm-sized sub-fractions were recovered from diluted fluids by flocculating the suspended matter with ultra-pure NaCl (1 M) and by removing the excess electrolyte by repeated centrifugation and dialysis.

Then, the nm-sized fractions were X-rayed to determine the mineral compositions and possibly to quantify the identified components. Each fraction was scanned twice: air-dried (AD) and after ethylene-glycol solvation overnight at 60°C (EG) (Table [1]; Fig. [2]). Small rock chips and crystal powders were coated with gold or carbon for scanning electron microscopic (SEM) and transmission electron microscopic (TEM) observations, respectively. The Ar extractions were completed in a glass line, following the method of Bonhomme et al. ([1975]) with a preheating step under vacuum in the extraction line at 80°C over a period of at least 24 h to remove as much as possible the atmospheric Ar adsorbed on the particles during preparation, separation, and handling. The K contents were measured by flame spectrometry with a routine precision better than 1.5 wt.% for amounts of K > 0.5 wt.%. To constrain as well as possible the K contents to this <0.5% limit, the aliquots were first screened for an approximate determination of their K contents, and then each was framed by internal standards set below and above the initially screened contents, the final contents being determined by interpolation between the three values at an estimated precision of 5 wt.%. The accuracy of the Ar extraction was checked weekly by measuring the international glauconite standard GL-O that averaged 24.59 ± 0.17 $(2\sigma) \times 10^{-6}$ cm^3/g (STP) radiogenic ^{40}Ar for five independent measurements during the course of the study,

which is within the recommended standard value of 24.85 ± 0.48 $(2\sigma) \times 10^{-6}$ cm^3/g (Odin et al. [1982]). The survey of the procedure also included periodic determinations of atmospheric $^{40}Ar/^{36}Ar$ loads that averaged 298.7 ± 1.2 (2σ), to be compared to the recommended value of 298.6 ± 0.4 (2σ; Lee et al. [2006]). Because of the expected small amounts of radiogenic ^{40}Ar due to small K_2O contents and potential young ages of the separates, the blanks of the coupled extraction line and mass spectrometer were also controlled before each Ar extraction. Their contents never exceeded 1×10^{-8} radiogenic ^{40}Ar, often being $<1 \times 10^{-9}$, which means that the equipment did not add measurable residual ^{40}Ar to that of the samples. Some of the ^{40}Ar analyses were also duplicated for further control of the equipment. The K-Ar ages were calculated using the recommended decay constants (Steiger and Jäger [1977]) with their usual analytical uncertainties (Table [2]). The isochron calculations were not given systematically with their corresponding 2σ errors because the individual uncertainties of some analyses were such that this precision was not always of real use.

The nm-sized sub-fractions of the A1 and B1 samples were also analyzed for their Rb-Sr isotopic systematics after supplementary, gentle acidic leaching. This leaching was maintained despite the initial removal of the exchangeable elements hosted by the smectite structure and adsorbed on the mineral surfaces at a coarser grain size, and of the elements released by the associated soluble minerals (Jackson [1975]). None of the reactive chemical products used added any of the measured elements as they were selected for their ultra-pure quality. In fact, this supplementary acidic leaching allows independent determinations of the Sr contents and $^{87}Sr/^{86}Sr$ ratios of the solid I-S particles and of the mobile counterparts around and within the I-S crystal agglomerates. These elements were recovered by gentle leaching of the sized fractions with ultra-pure dilute HCl (1 M) over a period of 15 min at room temperature followed by centrifugation (Clauer [1982]). This gentle acid leaching does not alter the Rb-Sr or the K-Ar system of the clay materials regardless of type, size, or degree of crystallization (Clauer et al. [1993]). The data points of the leachates (labeled L) also need to be aligned with those of the untreated (labeled U) and residual (labeled R) separates in an $^{87}Sr/^{86}Sr$ vs. 1/Sr diagram and occasionally in an $^{87}Sr/^{86}Sr$ vs. $^{87}Rb/^{86}Sr$ diagram, to substantiate a somehow delicate separation and an appropriate analysis. The significance of the arrays obtained depends strictly on the material studied; geologically meaningful 'isochrons,' for instance, can be claimed only if all of the material analyzed, liquid and solid, was demonstrated independently to be homogeneously authigenic. If this requirement is not fulfilled, the arrays or the scattered data represent mixtures of solids and solubles of different origins. After tri-acid digestion of the residues and evaporation of the leachates, the Rb and Sr elements were separated by resin chromatography and analyzed by mass spectrometry for their Sr contents and isotopic compositions. These data were obtained on a thermo-ionization mass spectrometer with a multi-collector of five mobile collectors, whereas the Rb elemental amounts were

Table 1. XRD data of the <0.02, 0.02–0.05, and 0.05–0.1 µm size fractions of the six selected bentonite samples

Sample ID	Illite-smectite				Other minerals			
	008 2θ	009 2θ	delta 2θ	(%) S in I-S	Discrete illite	Kaolinite	Dolomite	Pyrite + Marcasite
A1 <0.02	42.74	48.21	5.47	92	Tr			
A1 0.02–0.05	42.83	48.29	5.46	91	X			
A1 0.05–0.1	42.85	48.33	5.48	92	Xx			
A2 <0.02	42.79	48.33	5.54	94	tr?			
A2 0.02–0.05	42.85	48.42	5.57	95				
A2 0.05–0.1	42.87	48.48	5.61	96				
A3 <0.02	–	–	–	–	–			
A3 0.02–0.05	42.89	48.38	5.49	92			tr?	
A3 0.05–0.1	42.89	48.48	5.59	95	tr?	tr		
B1 <0.02	42.91	48.46	5.55	94				
B1 0.02–0.05	42.79	48.42	5.63	96		x		
B1 0.05–0.1	42.79	48.4	5.61	96	Tr	x		
B2 <0.02	42.89	48.5	5.61	96				
B2 0.02–0.05	42.85	48.44	5.59	95				
B2 0.05–0.1	42.81	48.44	5.63	96		tr		
B3 <0.02	42.83	48.38	5.55	94				
B3 0.02–0.05	42.85	48.46	5.61	96		x		
B3 0.05–0.1	42.85	48.5	5.65	97	Tr	x		tr?

determined on a second mass spectrometer with a single collector, both following a procedure described by Schaltegger et al. (1994). The reproducibility and precision of the analytical cycle were controlled periodically with the ^{87}Sr/^{86}Sr ratio of the NBS987 standard. Its ratio averaged 0.710257 ± 0.000015 (2σ mean) for four independent determinations during the course of the study, the internal uncertainty of each analysis being given at the 2σ level (Table 3). The ^{87}Rb/^{86}Sr ratio had a ±1% (2σ) internal analytical uncertainty and the Rb-Sr data were calculated with the usual decay and fractionation constants (Steiger and Jäger 1977). When realistic, the calculated analytical uncertainties of the alignments obtained were based on Ludwig's (2003) *Isoplot* program.

GEOLOGICAL SETTING

The Campos Basin represents, with the nearby Santos and Pelotas Basins, the rift-basin system of the southern Brazilian continental margin between 20°S and 24°S. This deposition center accumulated a stratigraphic succession up to 9 km thick comprising continental to deep-marine sediments intercalated with basaltic flows and ash levels. Limited to the north by the Vitória-Trindade Chain and to the south by the Cabo Frio High, the Campos Basin covers an area of 115,000 km² (Fig. 1a; Mohriak et al. 1990). Accounting for ~85% of the total hydrocarbon production of the whole area, it is a prolific hydrocarbon producer with oil hosted mainly by sandy turbidites. The structural and volcanic processes that contributed to the continental break-up and the tectonic-stratigraphic evolution of this complex sedimentary basin have been studied extensively (e.g. Kumar et al. 1977; Ojeda 1982; Chang et al. 1992; Cainelli and Mohriak 1999; Mohriak et al. 2002). The whole margin shows permanent changes in subsidence and in the sediment supply, both subordinated to the eustatic sea-level changes in a system controlled mostly by interconnected tectonic actions and sedimentary parameters. Of use for the present study is the burial-depth history of the Barremian to Holocene stratigraphic succession (Contreras 2011) that provides a temperature trend based on data collected at two locations in the basin (Fig. 1b). Also, seismic-stratigraphic data along horizontal seismic lines and in vertical drillings testify to the complexity of the sedimentary sequence (Fig. 1c).

Altered volcanic beds were described as interlaying the Upper-Cretaceous turbidites in the central Campos Basin (Alves et al. 1993; Viana et al. 1998) within shales and siltstones of the Ubatuba Formation and in sandstone reservoirs of the Carapebus Formation. Varying from 5 cm to 1 m in thickness, these bentonite beds occur mostly near the top of sandstone lobes (Caddah et al. 1998) with the thinnest layers, often bioturbated and mixed with the host shales. The tectonic activity associated with the volcanic episodes probably played a determining action by initiating the siliciclastic turbidite flows during the Santonian/Campanian epochs (Caddah et al. 1998). Six Santonian (85.8–83.5 Ma) bentonite samples buried to ~2800 m were collected from drill-cores for this study. The precise geographic location of the drillings and the detailed stratigraphic ages of the samples in the drill-hole(s) were not provided. The A1 sample was selected deliberately because of

Table 2. K-Ar data of the <0.02, 0.02–0.05, 0.05–0.1, and 0.1–0.2 μm size fractions of the six bentonite samples

Samples	K_2O (%) analyzed	K_2O (%) from XRD	rad. Ar (%)	rad. ^{40}Ar (10^{-6} cm^3/g)	$^{40}Ar/^{36}Ar$	$^{40}K/^{36}Ar$	Age (Ma ± 2σ)
Sample A1							
<0.02 μm	0.70	0.56	14.56	0.97	345.9	0.020	42.6 ± 3.2
0.02–0.05 μm	1.12	0.58	14.59	1.92	346.0	0.016	53.4 ± 4.5
0.05–0.1 μm	1.67	0.53	21.92	3.34	378.4	0.023	60.9 ± 2.9
0.1–0.2 μm	1.88	–	34.50	4.34	–	–	70.2 ± 2.1
Sample A2							
<0.02 μm	0.29	0.40	2.26	0.15	302.3	0.007	15.9 ± 7.5
duplicate		–	1.49	0.15	300.0	0.005	15.5 ± 10.7
0.02–0.05 μm	0.34	0.33	2.68	0.29	303.6	0.005	26.0 ± 11.6
0.05–0.1 μm	0.39	0.24	2.47	0.31	303.0	0.005	24.4 ± 10.2
0.1–0.2 μm	0.39	–	2.87	0.43	304.2	0.004	34.2 ± 12.0
Sample A3							
0.02–0.05 μm	0.42	0.51	0.38	0.57	296.7	0.000	41.3 ± 10.8
0.05–0.1 μm	0.42	0.29	1.82	0.54	301.0	0.002	39.7 ± 22.0
0.1–0.2 μm	0.42	–	4.43	0.58	309.2	0.005	42.3 ± 9.7
Sample B1							
<0.02 μm	0.30	0.38	1.93	0.19	301.3	0.005	19.3 ± 10.1
duplicate		–	1.64	0.31	300.4	0.002	31.8 ± 10.3
0.02–0.05 μm	0.26	0.20	1.64	0.17	300.4	0.004	20.6 ± 13.0
0.05–0.1 μm	0.35	0.24	10.09	0.53	328.7	0.012	46.6 ± 4.9
0.1–0.2 μm	0.38	–	7.29	0.70	318.7	0.007	56.2 ± 7.8
Sample B2							
<0.02 μm	0.26	0.24	0.0	0.00	294.9	0.002	0.0
0.02–0.05 μm	0.21	0.29	1.74	0.57	298.0	0.002	82.4 ± 47.2
0.05–0.1 μm	0.20	0.20	0.39	0.06	296.7	0.002	9.9 ± 27.0
0.1–0.2 μm	0.24	–	2.05	0.24	301.7	0.003	30.9 ± 15.2
Sample B3							
<0.02 μm	0.30	0.38	0.0	0.00	292.5	0.006	0.0
duplicate		–	0.0	0.00	292.4	0.004	0.0
0.02–0.05 μm	0.24	0.24	0.0	0.00	297.1	0.000	0.0
0.05–0.1 μm	0.25	0.15	3.53	0.45	306.3	0.003	54.6 ± 15.5
0.1–0.2 μm	0.33	–	4.02	0.54	307.9	0.004	49.7 ± 12.5

a visible contamination by the hosting turbidite for comparison of its mineralogical and isotopic data with those of the five other bentonite samples which were apparently not contaminated.

RESULTS

The Clay Mineralogy and Morphology

The mineral composition of all size fractions of <0.2 μm is dominated by a smectite-type mineral, as all air-dried patterns outline a strong XRD 001 reflection at ~12 Å (for one water layer) and its higher orders, whereas the ethylene-glycolated specimens show ~17 Å 001 reflection (for two glycol layers), again with its higher orders (Fig. 2). The amount of smectite layers in the I-S was evaluated by the most precise method

available based on the angular distance between the 008 and 009 reflections of smectite (Table 1; Środoń 1980). The precision of this measurement depends on the registration quality of the XRD patterns and has been estimated here as better than 2% of smectite layers. Traces of kaolinite were also detected in four samples, as well as traces of dolomite in one sample and of pyrite and marcasite in another sample (Table 1)

Identification of the smectite mineral in the <0.2 μm fractions of the six bentonites was based on the Δ2 peak position method of Środoń (1980) using the following experimental regression based on the data of Środoń et al.(2009a):

$$\%S = 2.6063 \times \Delta2^2 + 0.6258 \times \Delta2 + 10.282,$$

where Δ2 is the angular distance (°2θ CuKα) between the 008 and 009 illite-smectite reflections in the 42.5 – 48.5°2θ range

Table 3. Rb-Sr data of the untreated (Unt.), leachate (Leach.), and residue (Res.) separates from <0.02, 0.02–0.05, 0.05–0.1, and 0.1–0.2 μm size fractions of the samples A1 and B1

Samples	Rb (μg/g)	Sr (μg/g)	Rb/Sr	$^{87}Rb/^{86}Sr$	$^{87}Sr/^{86}Sr$ (±2σ in 10^{-6})	K/Rb
Sample A1						
<0.02 μm Unt.	21.16	9.03	2.343	6.781	0.712667 ± 11	137
Leach.	9.40	61.92	0.152	0.439	0.709713 ± 10	
Res.	32.07	4.41	7.272	21.08	0.719201 ± 15	
0.02–0.05 μm Unt.	34.06	25.00	1.362	3.943	0.711707 ± 16	136
Leach.	13.67	152.5	0.090	0.259	0.709785 ± 10	
Res.	37.02	10.12	3.658	10.59	0.715724 ± 10	
0.05–0.1 μm Unt.	45.21	38.26	1.182	3.421	0.711918 ± 10	153
Leach.	16.93	137.7	0.123	0.356	0.709748 ± 10	
Res.	46.11	21.65	2.130	6.167	0.714054 ± 13	
0.1–0.2 μm Unt.	49.89	60.99	0.818	2.368	0.711724 ± 10	156
Leach.	15.43	65.90	0.234	0.678	0.710284 ± 10	
Res.	38.60	29.22	1.321	3.825	0.713245 ± 10	
Sample B1						
<0.02 μm Unt..	6.74	18.25	0.369	1.069	0.709932 ± 10	185
Leach.	7.66	136.5	0.056	0.162	0.709791 ± 10	
Res.	10.49	4.10	2.559	7.412	0.711070 ± 11	
0.02–0.05 μm Unt.	7.44	14.41	0.516	1.494	0.710695 ± 10	145
Leach.	6.71	58.46	0.115	0.333	0.710800 ± 10	
Res.	9.78	7.87	1.243	3.596	0.711012 ± 9	
0.05–0.1 μm Unt.	10.07	24.48	0.411	1.190	0.710087 ± 10	144
Leach.	12.12	107.1	0.113	0.328	0.710758 ± 10	
Res.	10.90	14.05	0.776	2.245	0.709530 ± 13	
0.1–0.2 μm Unt.	11.19	33.95	0.330	0.963	0.709809 ± 12	144
Leach.	11.14	98.81	0.113	0.326	0.710555 ± 10	
Res.	12.17	22.72	0.537	1.550	0.709271 ± 11	

The uncertainty of the $^{87}Sr/^{86}Sr$ ratio is given in 10^{-6} at the 2σ/mean level.

(Table 1). All mineral fractions consisted of smectite-rich I-S containing from ~3% illite layers in a size fraction of sample B3 to 9% in a fraction of sample A1. The percentage of smectite layers (%S in Table 1) in the I-S was also used to estimate the corresponding expected K_2O content of the size fractions, assuming that all positions of fixed cations in the illite structure were filled with K (Środoń et al. 2009b). The following regression based on the experimental data of Środoń et al. (2019) for highly smectitic clays (>60 %S) was used:

$$\%K_2O_{XRD} = -0.0755 \times \%S + 7.4777.$$

The calculated K_2O contents corresponded well to the measured values (Table 2), while being less than those of the contaminated sample A1. The difference between the measured and the calculated K content in the A1 sample relates to the illite admixture shown by two independent ways. This result indicates that all analyzed K in the I-S is fixed, and that the contribution of ammonium is insignificant (e.g. Środoń et al. 2009a, b).

Observations by SEM at low magnification show irregular surfaces which appear to mimic the initial volcanic ash with large imprints of coarse original crystals in the 0.1 mm range (Fig. 3a). In detail, these rough surfaces consist of laminar crystal sheets at the edges of the ash particles (Fig. 3b). Perpendicularly, the sheets are organized into micrometer-sized lamellar "booklets" (Fig. 3c). At higher magnification, the 1-μm platy particles appear oriented, which suggests the action of a pore-fluid flow during crystallization of the particles (Fig. 3b). The TEM observations showed very thin, almost transparent particles with surfaces of about 1-μm² (Fig. 3d,e).

The K-Ar Data

The XRD data, together with the geochemical simulations of the K_2O contents in sample A1, confirmed the presence of independent illite crystals possibly occurring also in some of the A2, A3, B1, and B3 separates (Table 1). The calculations of the K_2O contents showed a reasonably consistent correlation with the measured K_2O contents (Table 2). Only those of sample A1 showed differences between the analyzed and computed K_2O contents due to the detrital illite, which implies
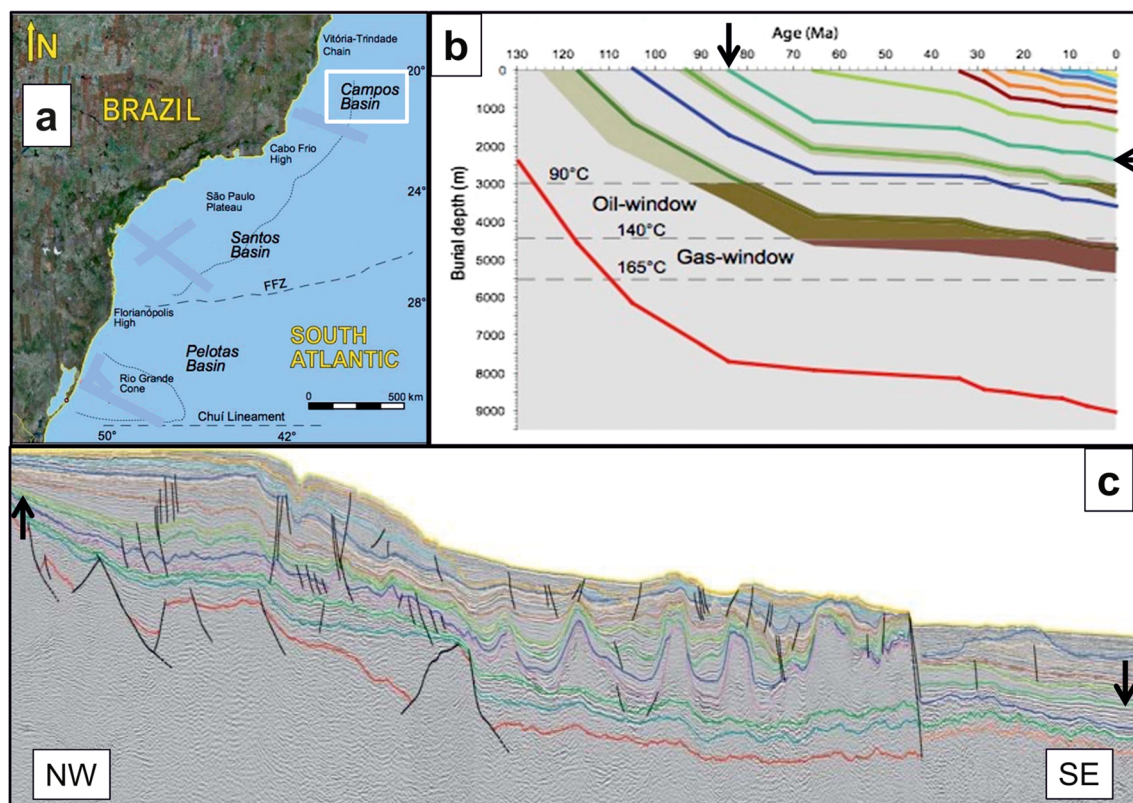
Fig. 1. a Map of the offshore southwestern margin of the South Atlantic Ocean on the Brazilian continental margin with the location of the Campos Basin; **b** sketch of the burial-depth curve of the volcano-sedimentary sequence. The layers of the studied bentonites are indicated by the arrows; and **c** a profile of the turbidite system along the offshore, again with the arrows marking the bentonite layers (the three sketches are reproduced, with the permission of the author, from Contreras 2011)

that the K of the I-S is held strongly enough by the so-called fundamental particles to be dated by the K-Ar method. The Rb-Sr method based on the disintegration of Rb, the 'sister' element of K, is theoretically also applicable because Rb yields similar characteristics to K but at much smaller amounts. The K_2O contents of samples A1 and A2 increased with particle size, while remaining stable in the A3 and B2 samples. The few duplicated analyses showed either identical data in the case of the <0.02 μm fractions of samples A2 and B3, or values within analytical uncertainty in the case of the <0.02 μm fraction of sample B1.

The individual K-Ar results were divided into four groups, not taking into account the data of the 0.05–0.1 μm size fractions of the A3 and B2 samples and that of the 0.02–0.05 μm fraction because of their excessive analytical uncertainties. Three fractions of sample A1 yield K-Ar data beyond 53 Ma, together with one fraction of sample B1 and two fractions of sample B3. As the XRD diagrams of the coarse size fractions confirmed the occurrence of detrital illite, these higher isotopic data have no geological meaning. The smallest separate of samples A1, all those of the samples A2 and A3, and the two smallest of sample B3 yielded data between 47 and 16 Ma, comprising a group of values within analytical uncertainty for all the fractions of sample A2, while those of sample B3

increased slightly with grain size, which could also relate to some contamination by detrital illite. The third group included intermediate fractions of samples A2, B1, and B2 with data between ~10 and 26 Ma, comprising also the smallest fractions of samples B2 and B3 that are characterized by very small amounts of K_2O and even by the lack of radiogenic ^{40}Ar. By considering again the large analytical uncertainty, the samples of this third group yielded K-Ar data ranging from 0 to ~26 Ma. No contaminant minerals other than apatite and dolomite that theoretically do not affect the K-Ar values could be detected in the separates. Note also that all K-Ar data obtained were systematically below the stratigraphic age of the bentonite beds, even those of sample A1 with the detrital illite.

Often used in K-Ar dating of clay minerals, Harper's (1970) diagram visualizes well the relationship between the K_2O and radiogenic ^{40}Ar contents of the analyzed materials. Except for the data points of the four size fractions of sample A1, all others scattered narrowly between 0.2 and 0.4% K_2O and between 0.0 and 0.6×10^{-6} cm^3/g of radiogenic ^{40}Ar (Table 2; Fig. 4a, Fig. 4b). In the alternative isochron diagram, most available data points were clustered at the lower, left part of the diagram (Fig. 6a). Five of these size fractions plotted above the line joining the origin of the coordinates and the data point of the <0.02 μm fraction of sample A1 without detrital illite (Fig. 4b), while 13 more data
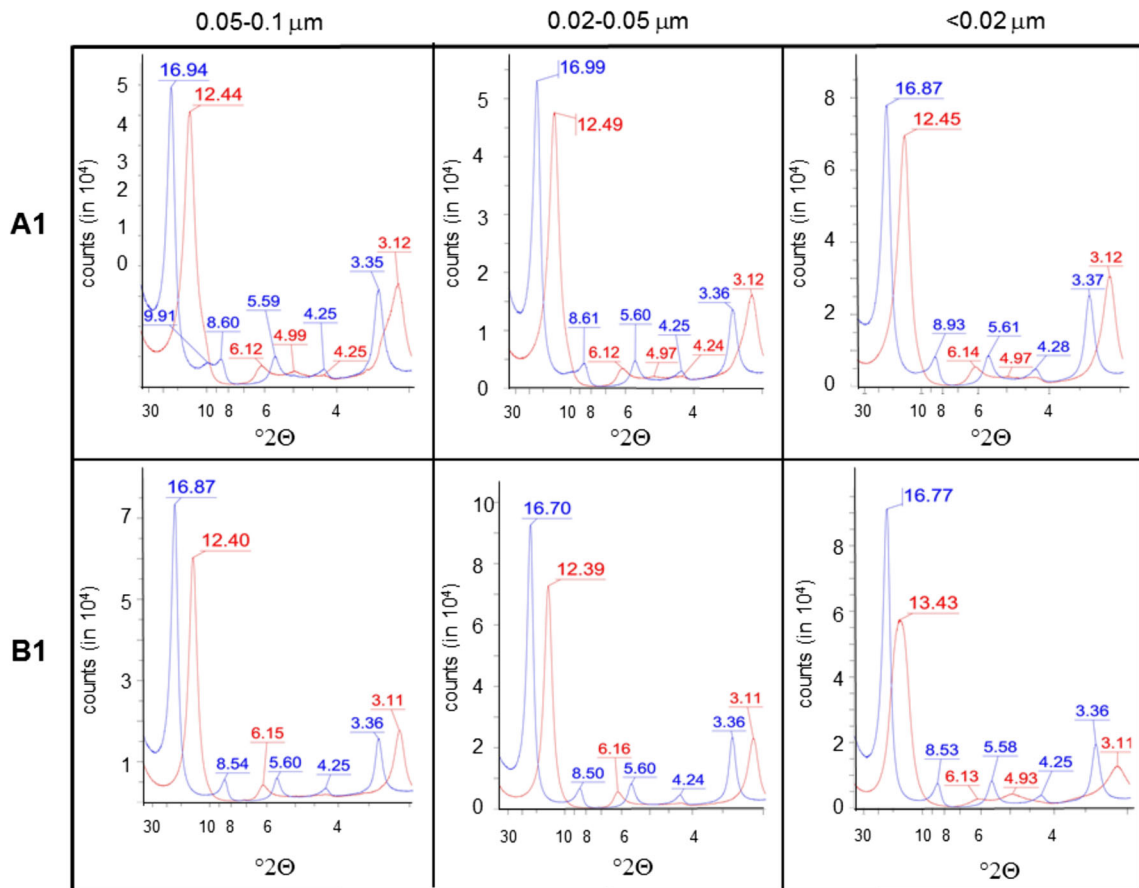
Fig. 2. XRD diagrams of the nm-sized <0.02, 0.02–0.05, and 0.1–0.2 μm size fractions of the A1 and B1 samples. The untreated air-dried separates are in red and the ethylene-glycolated separates are in blue

points plotted below that line and one on it. Interestingly, the size fractions with the smallest radiogenic ^{40}Ar did not plot near the intersection of the two coordinates, as they should have, but instead near the 0.2% K_2O content for 0% radiogenic ^{40}Ar. Relative to this display, the data of the A2 and B1 samples also trended more toward larger K_2O contents than expected relative to their radiogenic ^{40}Ar contents. Both correlations suggested that the smallest nano-sized illite crystals yield a depleted radiogenic ^{40}Ar content relative to the K_2O content, unless they contain an abnormally large K_2O content for no radiogenic ^{40}Ar. Independently, the data for the <0.02 and 0.02–0.05 μm fractions of sample B1 ranged from 19 to 31 Ma with large analytical uncertainties of 10 to 13 Ma, while those of the coarser 0.05–0.1 and 0.1–0.2 μm fractions scattered from 47 to 56 Ma, but with lower analytical uncertainties of 5 to 8 Ma, respectively. The data points for the two finest fractions fit a line intersecting the coordinates at their origin in a Harper diagram (Fig. 5a). This repartition favors a geological meaning of the K-Ar data, whereas the two coarser fractions fit a second line intersecting the ordinate at a negative value, which clearly does not support a meaningful age (Fig. 5b).

Among the eight other data points clustering in the Harper (1970) diagram, those above the horizontal segment through the origin can be considered as containing radiogenic ^{40}Ar in excess by 0.4×10^{-6} cm^3/g relative to 0% K_2O, whereas those below yield

an apparently average deficit of 0.5×10^{-6} cm^3/g of radiogenic ^{40}Ar relative to 0% K_2O, unless it is an excess of K_2O relative to 0×10^{-6} cm^3/g ^{40}Ar (Fig. 4b). A straight interpretation for this alternative possibility could, of course, be the loss of radiogenic ^{40}Ar due to grain-size decrease which has not been demonstrated. If this is the case, however, it cannot be due to a decrease in the size of the nano-sized crystals as the 0.1–0.2 μm size fractions of the B1 and B2 samples are among these separates. Those on the horizontal coordinate correspond to 0×10^{-6} cm^3/g ^{40}Ar and a narrow 0.24 to 0.30% K_2O.

The display of the individual data in an isochron diagram represents another solid validation test for the K-Ar dating method. However, its use implies restrictions that limit a straight application to clay minerals, as it requires a fair knowledge of the amount of atmospheric ^{36}Ar carried by any analyzed material to consolidate best the evaluation of the radiogenic ^{40}Ar. Because the amount of atmospheric Ar increases quite easily in clay samples by adsorption during sample handling and preparation, the ^{40}Ar/^{36}Ar ratio stored in the samples can be more or less biased with its impact on the final age. This adsorption aspect is well known: atmospheric Ar is removed routinely from clay minerals by pre-heating under vacuum, as was done in the present study. The radiogenic ^{40}Ar detected in the total contents of ^{40}Ar represents
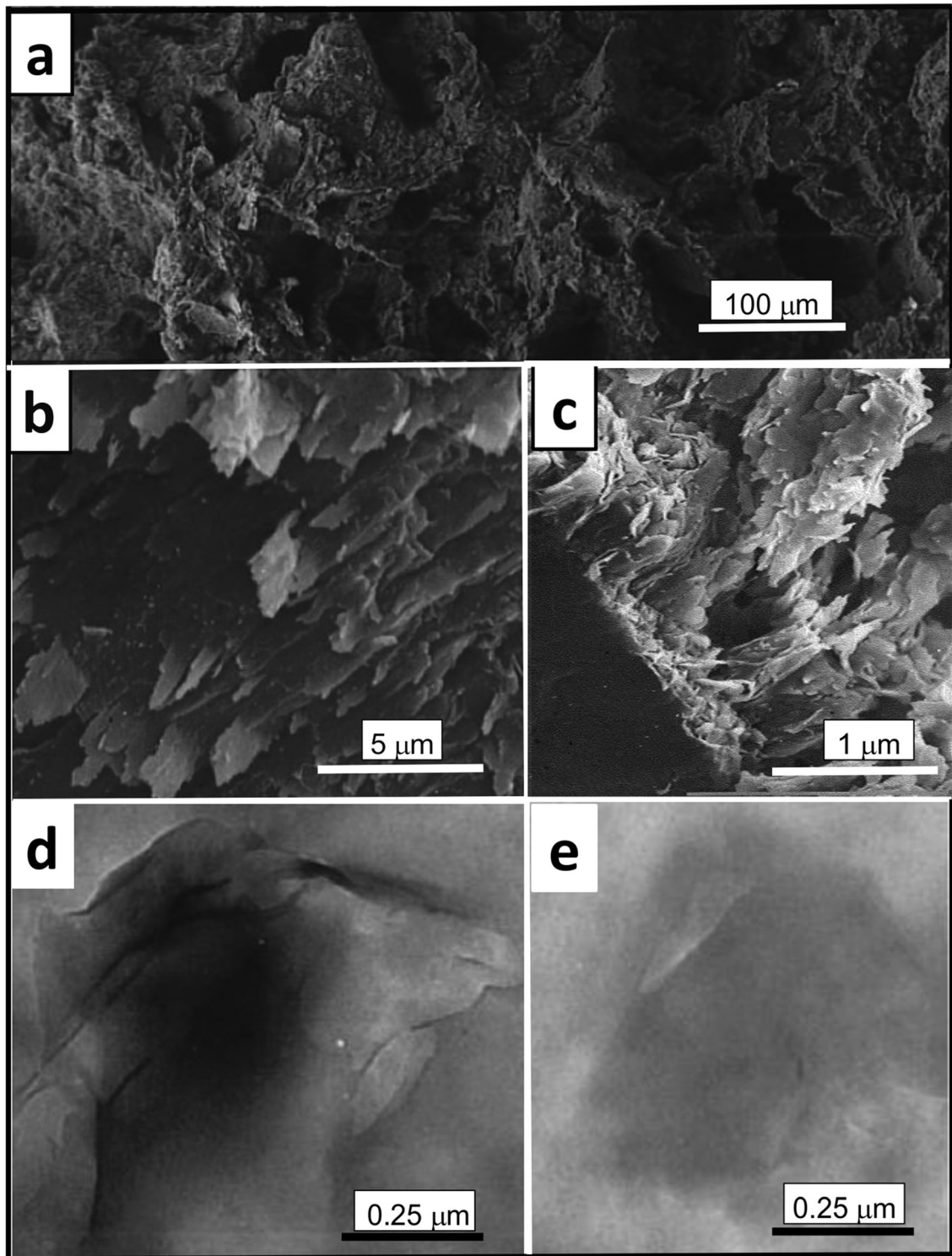
Fig. 3. SEM images of: **a** the bentonite sample A1 with some impacts of initial volcanic minerals; **b** sample A2 with authigenic illite-smectite crystals; **c** a closer look at a layer with very thin, irregular crystals relative to their surface; (**d, e**) TEM images showing very thin smectite crystals (apparently rolled in **d**)
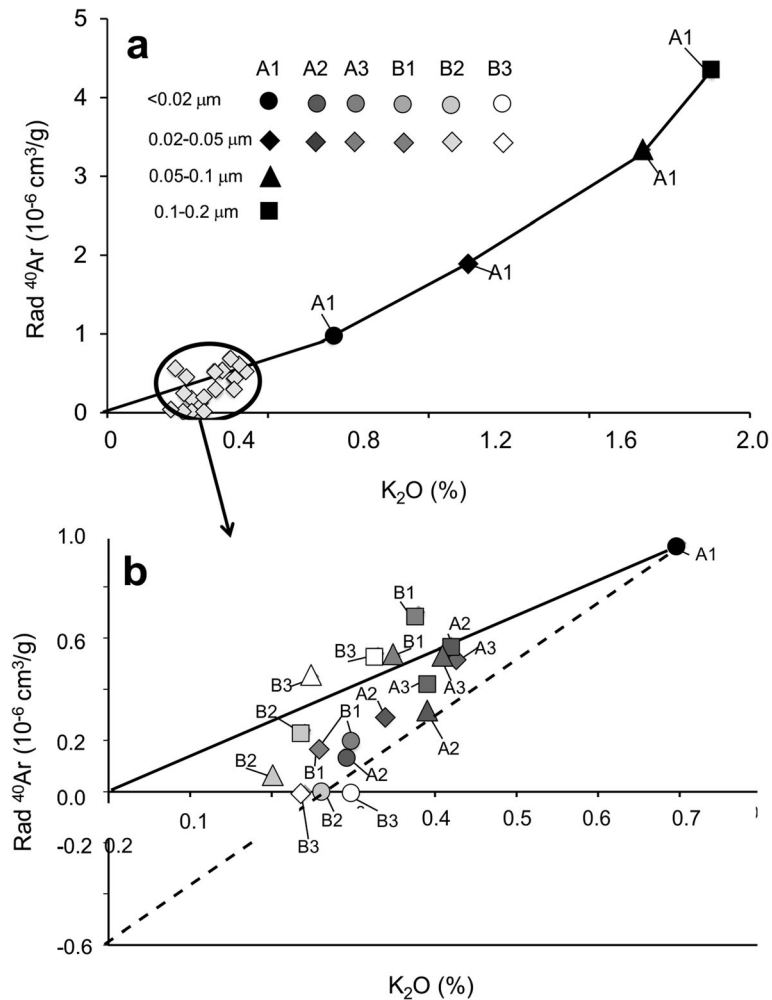
Fig. 4. a A Harper ([1970](#)) diagram with the plots of the size fractions from A1, A2, A3, B1, B2, and B3 samples and **b** enlargement of the data from A2, A3, B1, B2, and B3 samples (those of sample A1 were not redrafted here)

from 0.0 to 34.5% of the total measured ^{40}Ar in the size fractions analyzed (Table [2](#)), which is what was expected for young materials with small K contents but which is too small for a straight application of the isochron technique. As this amount of atmospheric ^{40}Ar could not be reduced in the I-S due to small K_2O contents and young ages, its ^{40}Ar/^{36}Ar ratio was checked carefully as it may bias the K-Ar data with a value which is somewhat distant from the atmospheric ^{40}Ar/^{36}Ar ratio. The check was obtained by means of the data for the fractions without detectable radiogenic ^{40}Ar and by the controls of the purified atmosphere splits. The four separates without radiogenic ^{40}Ar yielded an average ^{40}Ar/^{36}Ar ratio of 294.2 ± 2.9 (2σ), while the ^{40}Ar/^{36}Ar ratio of the atmospheric Ar measured during the course of the study was 298.7 ± 1.2 (2σ), both to be compared to the reference at 298.6 ± 0.4 (2σ; Lee et al., [2006](#)). The analytical coherence among the three results is such that a cautious use of the isochron method can be adopted except for the data with very large uncertainties.

The data points scattered along four lines in the isochron pattern (Fig. [6a](#)). That with the steepest slope integrated the two intermediate size fractions of sample A1 and four data points from the cluster in the lower left corner of the diagram (Fig. [6b](#)). This steepest line intersected the ordinate below the atmospheric ^{40}Ar/^{36}Ar value at ~288.8 ± 3.9. Most of these data points belonged to the coarsest fractions with two data points of sample B2 and two of sample A1 characterized by some detrital illite also visualized in the Harper ([1970](#)) diagram (Fig. [5a](#)). Together with the initial value of the line clearly below the atmospheric ^{40}Ar/^{36}Ar, this display suggests a mixing line with no geological meaning. The second line with two data points outside the cluster and four to five data points from the cluster yielded an average age of 45.9 ± 11.0 Ma and an intercept at 296.9 ± 0.2 within the analytical range of the atmospheric ^{40}Ar/^{36}Ar value. Due to the large individual uncertainties for most K-Ar data of these size
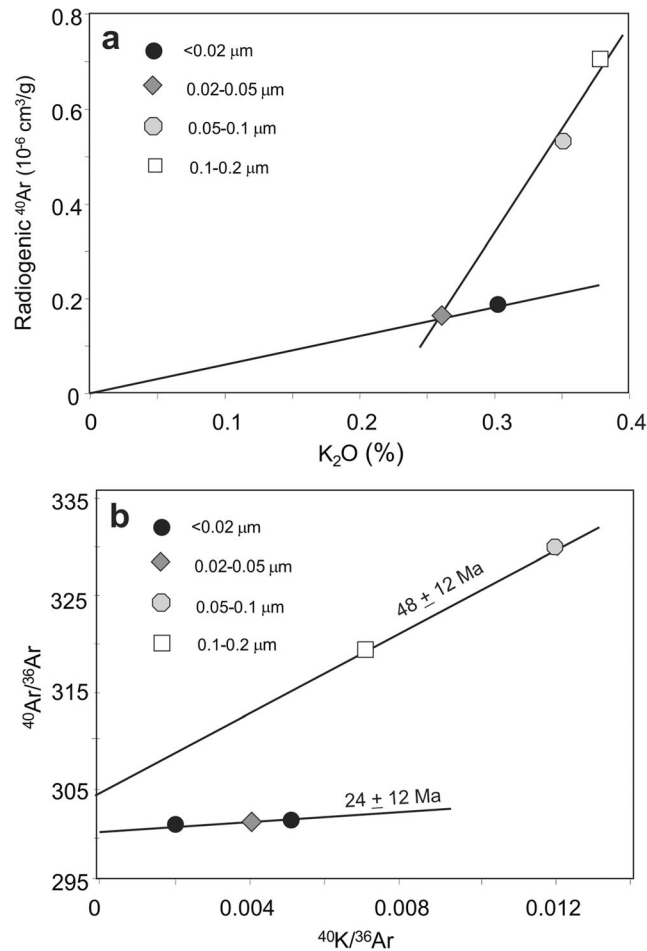
Fig. 5. a A Harper (1970) diagram and **b** a more detailed plot of the same pattern with all analyzed size fractions of sample B1

fractions, a more precise error calculation was considered inaccurate. Despite these individual uncertainties, the line satisfies the prerequisites of an isochron with an age that might be a milestone in the evolution of the smectite-rich I-S. Some discrete detrital illite cannot be excluded formally in some of the size fractions concerned, however, on the basis of the XRD information. Of the remaining data points, five fit a third alignment with an even less steep positive slope and with the same initial $^{40}Ar/^{36}Ar$ ratio than the previous one. The characteristics of the line were, as for the previous one, calculated routinely with an age value at 10.9 ± 5.5 Ma based on the same initial $^{40}Ar/^{36}Ar$ ratio of 296.9 ± 0.2. This analytical choice was justified by the large individual uncertainties and by the presence of two samples at the origin that could not be related with certainty to any of the two groups of data.

The data in the two smallest size fractions of the B2 and B3 samples plotted along a supplementary line with an initial $^{40}Ar/^{36}Ar$ value equal to that of the atmosphere and a slightly negative slope (Fig. 6b). This scatter with values below the analytical uncertainty of the atmospheric $^{40}Ar/^{36}Ar$ was probably due, at least partly, to the analytical performance of the mass spectrometer that might be at its limits. In fact, the

atmospheric $^{40}Ar/^{36}Ar$ ratio was never below the theoretical value published, e.g. by Lee et al. (2006). Analysis of unspiked samples (e.g. Gillot and Cornette 1986) could have been a plausible complementary or alternative test of the analytical aspect, but whether that would have been the case is doubtful, as the $^{40}Ar/^{36}Ar$ atmospheric ratio obtained provided an acceptable resolution. It would probably not have helped to evaluate directly the relative contents of the radiogenic and the atmospheric ^{40}Ar in the size fractions.

In summary, K-Ar ages were obtained at 45.9 ± 11.0 and $10.9 + 5.5$ Ma, with a large analytical uncertainty for the older age. The K-Ar data also highlight the occurrence of nm-sized illite layers lacking radiogenic ^{40}Ar. Some of the size fractions yielded $^{40}Ar/^{36}Ar$ ratios slightly below the atmospheric value. The lack of radiogenic ^{40}Ar could not be shown to have resulted from its loss from the nm-sized I-S, or from a very recent supply of K that had not yet decayed to radiogenic Ar, which would explain the 0 Ma age.

The Rb-Sr Data

The Rb contents of the untreated (labeled U) size fractions increased in sample A1 from 21 to 50 μg/g when the particle size increased, and significantly less, from 6.7 to 11.2 μg/g, in
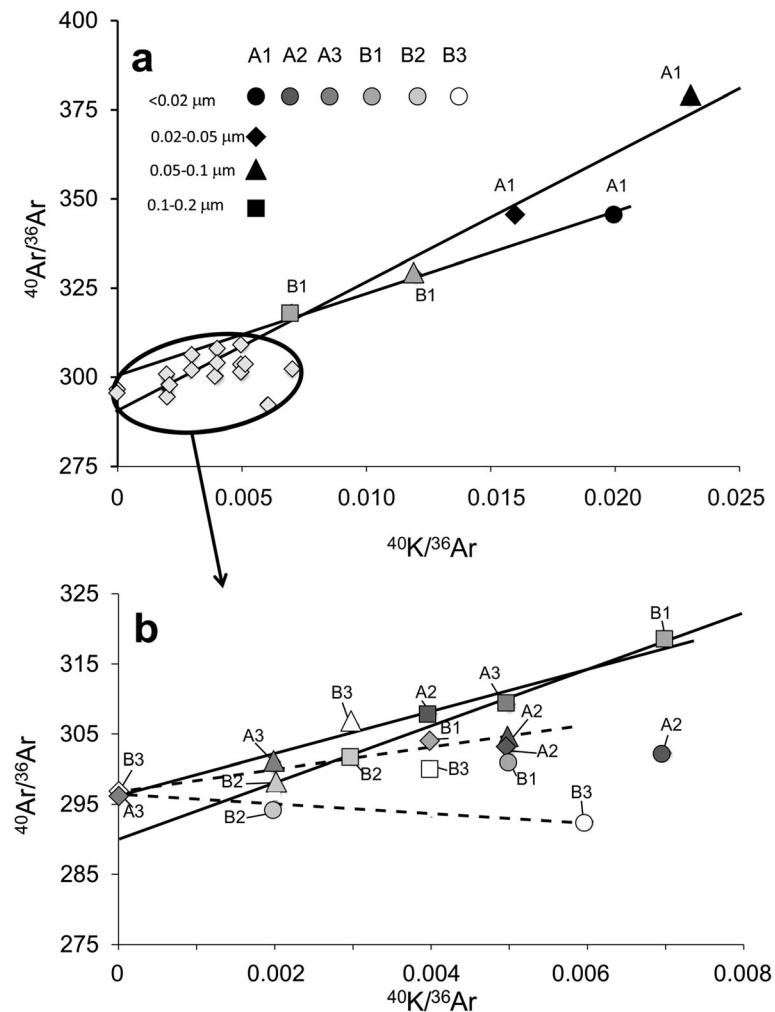
Fig. 6. An isochron $^{40}Ar/^{36}Ar$ vs. $^{40}K/^{36}Ar$ plot of the different size fractions of the samples A1 and B1. Part **b** is an enlargement of part **a**

sample B1 (Table 3). The Sr contents increased also with increasing particle size for both the A1 and B1 samples from 9.0 to 61.0 μg/g and from 18.3 to 34.0 μg/g, respectively. The Rb/Sr ratio increased from 0.82 to 2.34 in sample A1 when grain size increased, remaining almost constant in sample B1 from 0.33 to 0.37. The $^{87}Sr/^{86}Sr$ ratio decreased slightly from 0.7127 to 0.7117 in the untreated separates when grain size increased in the fractions of sample A1, while remaining constant at 0.70100–0.70107 in those of sample B1.

The Rb contents of the leachates (labeled L) increased irregularly with grain size from 9.4 to 15.4 μg/g in sample A1 and from 7.7 to 11.4 μg/g in sample B1. The Sr contents were also variable with the greatest values in the intermediate size fractions of sample A1 and in the coarser fractions of sample B1. Consequently, the Rb/Sr ratio remained small from 0.06 to 0.12. The $^{87}Sr/^{86}Sr$ ratios, still of the leachates, were fairly constant in the fractions of sample A1 at ~0.7097–0.7103, whereas they were slightly higher at 0.7106–0.7108 in those of sample B1. The lower values were slightly above the average value of modern seawater that is set at 0.70919 ± 0.00001 (Hodell et al. 1990).

The Rb contents of the residues (labeled R) were fairly constant for the sub-fractions of both samples from 32.1 to 46.1 and from 9.8 to 12.2 μg/g, respectively. The Sr contents increased from 4.4 to 29.2 μg/g in the leachates of sample A1, and from 4.1 to 22.7 μg/g in those of sample B1 when grain size increases.

As a preliminary result, all L-U-R data points of each size fraction plotted straight on their respective arrays, as expected in the case of a mastered separation (Clauer 1982; Clauer et al. 2011) with initial values close to the $^{87}Sr/^{86}Sr$ ratios of the leachates. These initial $^{87}Sr/^{86}Sr$ ratios ranged from 0.70951 ± 0.00015 (2σ) for the array of the <0.02 μm fraction to 0.70955 ± 0.00013 for that of the 0.02–0.05 μm fraction, to 0.70937 ± 0.00015 for that of the 0.05–0.1 μm fraction, and to 0.70985 ± 0.00017 for that of the 0.1–0.2 μm fraction, which together were within analytical uncertainty at 0.70957 ± 0.00024 (2σ). The L-U-R data points of the four A1 size fractions plotted along four individual arrays in an $^{87}Rb/^{86}Sr$ vs. $^{87}Sr/^{86}Sr$ isochron pattern with slopes decreasing with the size of the fractions (Fig. 7). Those of the four B1 size fractions outlined a more complex pattern: the data points of the finer <0.02 and 0.02–0.05 μm fractions fit along two lines with
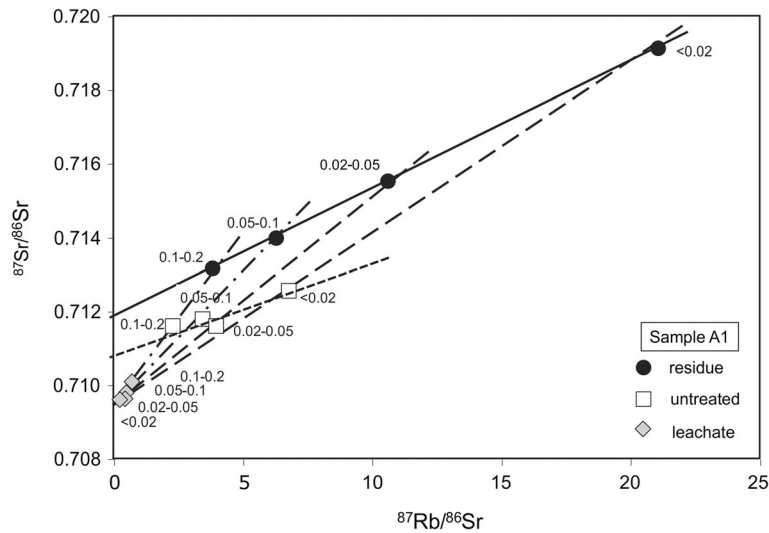
Fig. 7. A Rb-Sr data plot of the untreated, leachate, and residue separates of each size fraction of sample A1

positive slopes, whereas the coarser 0.05–0.1 and 0.1–0.2 μm triplets fit two lines with negative slopes (Fig. 8). In the latter case, the $^{87}Sr/^{86}Sr$ ratios of the leachates were greater than those of the corresponding residues, which is a seldom-seen spread of strictly sedimentary environments, but which has been reported in oceanic volcano-sediments (Clauer et al. 2011). The two L-U-R lines with the positive slopes yielded characteristics of isochrons giving close age values at 9.9 ± 4.2 and 12.5 ± 1.8 Ma with initial $^{87}Sr/^{86}Sr$ ratios of 0.71050 ± 0.00026 for the lower isochron and 0.70975 ± 0.00011 for the upper one. The lines through the U and the L data points characterize heterogeneous components and are, therefore, mixing lines. Also, the data points of the two coarser residues fit a further line giving an age of ~26 Ma with an initial

$^{87}Sr/^{86}Sr$ ratio of ~0.7087, both with large analytical uncertainties. In summary, the data points of the two finest residues of sample B1 plotted on two sub-parallel isochron lines giving an age of 10–12 Ma. Those of the two coarser residues plotted on a separate isochron line; only through two data points, however, with an age of ~26 Ma.

DISCUSSION

The Thermal Evolution and some Chemical Characteristics of the Bentonites

The nano-sized fractions of the selected bentonite samples consist overwhelmingly of a smectite type with a few illite
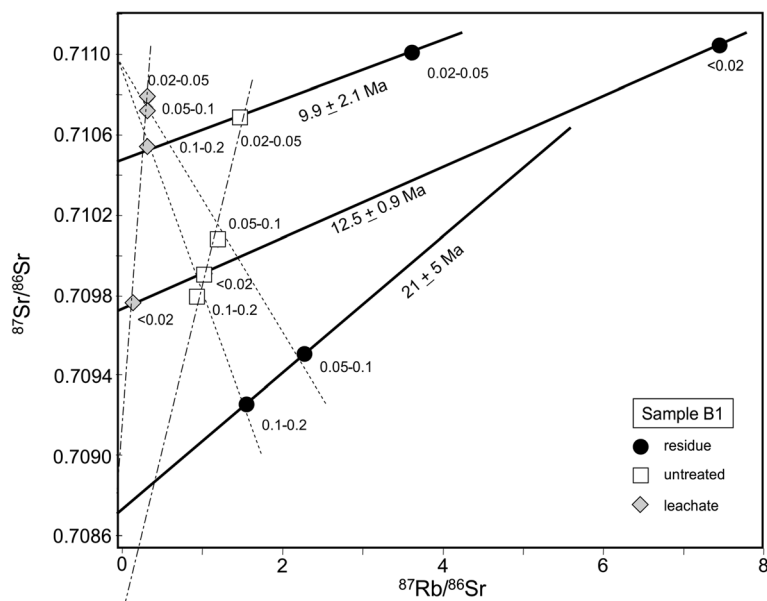

Fig. 8. A Rb-Sr data plot of the untreated, leachate, and residue separates of each size fraction of sample B1

layers, together with traces of detrital illite in sample A1, and kaolinite plus pyrite/marcasite in some of the other size separates. The small amount of authigenic illite suggests an overall small temperature increase during the thermal evolution of the ash layers, together with a very limited supply of K. The available depth/temperature modeling of these Campos bentonites consists of three successive, quite linear trends from a theoretical 0°C at the time of deposition at ~85 Ma, to 40°C about 20 Ma later, then to 50°C another 15 Ma later, and finally to 80°C now at a depth of 2300 m, the atmospheric temperature having not been taken into account (Fig. 1b; Contreras 2011). The bentonite samples studied were recovered at a present-day depth of ~2800 m, their location being apparently outside the available seismologic section. By correcting the temperature increase relative to the deeper sample location and by allowing 15°C for the atmospheric contribution, the bentonites studied were probably subjected to a final, present-day temperature of ~85°C. This value assumes a theoretical geothermal gradient close to 37°C/km, which is within the 24 to 41°C range of Cardoso and Hamza (2014) in the same area. It can, therefore, be agreed that the samples were subjected to a moderate diagenetic process.

Combining the K and Rb contents of the smectite-rich fractions may provide information about the type(s) of fluids involved in the smectite (and I-S) authigenesis, as used first by Turekian and Wedepohl (1961). The K/Rb ratio varied here between 136 and 185 for the untreated separates of the A1 and B1 samples. Relative to a value of 325 attributed by Elliott and Haynes (2002) to bentonite clays for diagenetic interactions of illite-rich I-S from the Appalachian bentonites with saline fluids, the low values obtained here discard an interaction with such saline fluids and agree with the overall limited degree of illitization.

The Rb-Sr System of the Smectite-rich I-S

Before discussing the behavior of the Rb-Sr isotopic system of the I-S materials, recalling that some of the interpretations may remain somewhat hypothetical would be appropriate. This statement is due to the limited number of samples and also to the limited amount of geographic and recovery information of the sampling, while the data confirm the mixing of authigenic and detrital illite in, at least, the two coarser size fractions of sample A1. Remember also that increasing array slopes through the data points of several size fractions in an isochron diagram means generally, when the grain size increases, that at least some of the size fractions are isotopically heterogeneous, and that the coarser size fractions contain more radiogenic ^{87}Sr and, therefore, 'older' crystals of detrital or depositional origin, as is the case here for the bioturbated sample A1. On the other hand, the narrow scatter of the initial ^{87}Sr/^{86}Sr ratios of the U-R-L triplets at 0.70957 ± 0.00024 (2σ), as is also the case here, suggests often that the mineral crystals of different size separates were in contact with pore fluids having similar to identical ^{87}Sr/^{86}Sr ratios. This value raises a problem about the true origin of the elements recovered here in the leachates by gentle dilute acid. The gentle acid leaching was completed after Jackson's (1975) treatment that can be considered to be rough enough to remove all elements

adsorbed at the surface of the crystals, together with the dissolution of any soluble mineral. The elements concentrated in the leachates could, then, probably result from a discrete disaggregation of crystal edges in contact with the gentle acid because of being less strongly bound than inside the crystals. Suggested by Thompson and Hower (1973) and Aronson and Douthitt (1986), this interpretation is based on experiments that were designed to study the behavior of K and Rb and of their daughter Ar and Sr isotopes of clay materials. In this case, the ^{87}Sr/^{86}Sr ratios of the leachates do not identify seawater or pore fluids.

The data points of the four residues (R) of sample A1 also plotted along an upper array that yielded an age of 24.3 ± 1.9 Ma (2σ) for an initial ^{87}Sr/^{86}Sr ratio of 0.71196 ± 0.00033 (2σ). In fact, this display does not suggest a decreasing occurrence of older minerals when grain size decreases, as the individual isotope data would rather plot along a hyperbolic trend as for the K-Ar system (Fig. 5a). Therefore, this 24-Ma value could result from aggregation of heterogeneous residues and would, then, not represent a reliable age step of the few authigenic illite layers from bentonites. However, it was also obtained independently by the K-Ar method on the two finer fractions of the same sample A1, of another fine fraction, and of a duplicate. The ambiguity of the K-Ar data is the location of the 0.02–0.05 μm data point on the two arrays. No clear interpretation can be provided for this 24-Ma record because of this ambivalence.

In this context, the negative slopes of the arrays by the two coarser 0.05–0.1 and 0.1–0.2 μm triplets of sample B1 (Fig. 8) raise concerns about the identity and the origin of the solid materials and about their interaction with pore fluids. Of sedimentary origin, the environmental fluids that may have interacted with the smectite crystals derived from volcanic ash and/or directly from hosting turbidites. Besides the hypothetical origin of the interacting fluids and the significance of the two slopes, it can be agreed that the analytical conditions were appropriate as the data points of the four L-U-R triplets all fit along straight lines.

In summary, illitization occurred after smectitization, apparently long after ash deposition (at ~85 Ma), unless the limited illitization was a 'side effect' of the overwhelming smectitization due to a very limited occurrence of K and Rb in the sedimentary pore fluids. In both cases, illitization was extremely limited with almost no Rb (or K) fixed in illite-type interlayer sites, a consequence being also that almost no radiogenic ^{87}Sr accumulated. The ^{87}Sr/^{86}Sr ratios of the leachates probably correspond to Sr somehow removed from crystal edges with values between 0.7106 and 0.7108, which is greater than those in the marine environment (Jones and Jenkyns 2001), either during ash deposition or later during illitization. Smectitization seems to have been fed, probably, by an aqueous environment that hosted Sr and moved through the pore system of the turbidites.

The K-Ar System of the Illite Layers in the Smectite Particles

Illitization has often been considered as a continuous process lasting, in progressively buried sediments and associated bentonite units, as long as temperature is increasing as shown,

e.g. in the East Slovak Basin (e.g. Šucha et al. 1993; Clauer et al. 1997). Such continuity depends on the local conditions in any sedimentary basin and on the supply of K by the pore fluids and can, therefore, be interrupted or even stopped. The burial/depth sketch used here has shown that the environmental temperature was lowest at the deposition of the ash layers and that it increased continuously until very recently. This evolution suggests, therefore, that illitization followed smectitization when the ambient temperature reached the appropriate level and that it might have continued since. In fact, no determining argument has been presented to favor either: (1) 'true' isotopic ages for the different size fractions of a sample when the process stopped definitively; or (2) successive steps of an ongoing process that corresponds to relative amounts of initial and final authigenic materials during a continuous crystallization, especially if its intensity increased with the temperature.

Knowledge of the regional evolution of the Campos Basin is not precise enough here to consolidate the isotopic data into geologically meaningful ages because of the unknown location of the samples and the quite linear increase in the temperature that sets at ~40 Ma the timing for its crossing of the 60°C level at which illitization starts. Also, if the process had stopped in any of the samples, the data of the smaller nano-sized fractions should be similar, indicating in turn the end of the process. Alternatively, the process seems to have been active up to now, with the isotopic data of some of the smallest fractions trending toward 0 Ma. By combining these constraints, the meaningful ages concentrate at ~45 and 0 Ma and, consequently, the coarsest size fractions of the B1 and B3 samples, together with the coarser A1 fractions yield meaningless data. From data of the smallest nano-sized fractions, the age span from 24 to 12 Ma could also yield a true age range for the A2 and B1 samples. If illitization is considered to be a continuous process powered by increasing temperature with possible stops depending on temperature variations and possibly K supply, it is very plausible that the data obtained either by groupings of individual data or alignments could report on content averages of 'older' relative to 'younger' particles and not on 'strict' ages. In turn, the values between the older 45 Ma and the younger 0 Ma would then depend on the specific mixing of the two generations and could, then, outline instead time intervals of illitization rather than age steps.

How did Smectitization and Illitization Proceed?

An overwhelming smectitization of volcanic glass occurred in the bentonite levels, but whether the K supply to the illite layers was supplied contemporaneously or later, when temperature was adequate and K available, is unclear. Indeed, it cannot be argued that the very small amounts of K in the I-S particles resulted from a limited supply by interacting K-poor pore fluids during the initial smectitization or from a later limited supply during an independent illitization. No indisputable evidence was found for contemporaneous or successive episodes from either of the isotopic dating methods as they apply solely to crystal interlayers with fixed K and its sister element Rb. The only age references are, therefore, from illite

layers even if they represent <10% of the overall smectite-rich particles. Moreover, the very limited occurrence of alkalis in the smallest nano-sized I-S separates and the small amount of radiogenic ^{40}Ar suggest that discrete illitization has probably occurred up to the present day.

The Smectite-to-illite Genetic Trend during the Evolution of the Campos Basin

Ash layers were deposited during Santonian time, between 85.8 and 83.5 Ma. They appear to have undergone a diagenetic episode that allowed dissolution of the volcanic glass and precipitation of authigenic smectite. During progressive burial, illite layers began to form by locking K and Rb into the crystalline structure. The combined K-Ar and Rb-Sr methods provide age milestones at 44 ± 4 Ma, 25–30 Ma, 12 ± 2 Ma, and probably between 2 and 0 Ma as potential steps in the illitization process. At this point, these isotopic ages validate the evolution of either a lasting but changing diagenetic event, or successive episodes that may have stopped somehow.

Smectitization of the ash deposits probably started when the environmental conditions favored an alteration (dissolution) of the ash particles, sketched at least by the different amounts of the two smaller and the two coarser nano-sized fractions of sample B1. All data points of their residues fit an isochron line with an initial ^{87}Sr/^{86}Sr ratio of 0.7120 ± 0.0003 (2σ; Fig. 7). These smectite-rich size fractions are not in isotopic equilibrium with the ^{87}Sr/^{86}Sr ratio of the leachates at 0.7096 ± 0.0002 (2σ). The scenario is different in the case of the B1 sample for which the two smallest and the two coarsest nano-sized fractions yielded different results, unless they represent different steps of a common evolution. The two smallest fractions gave similar ages for their L-U-R assemblages at ~12 Ma, but with significantly different initial ^{87}Sr/^{86}Sr ratios of 0.7097 and 0.7105. The components of the two coarser nano-sized fractions had obviously less interaction with pore fluids, as the residues still yielded a volcanic Sr isotopic signature. The leachates again yielded ^{87}Sr/^{86}Sr ratios at 0.7108 and 0.7105, close to those of the leachates removed from smaller size fractions. As no change in the sedimentation conditions can be suspected because of the lack of information, an alternative interpretation is needed to explain the differences among the solid separates of the same B1 sample. At this point, the coarser size fractions consist either of pure smectite crystals that crystallized from shards of the ash levels or of altered volcanic remnants mixed with authigenic smectite crystals, including the illite layers. None of the results available favors either of these hypotheses yet. With respect to the timing of the process(es), changes such as crystallization of smectite on volcanic ash could have started at ~45 Ma, and could have lasted for 20 Ma. Interestingly, the Rb/Sr ratios of the nano-sized smectite are systematically highest when grain size decreases (Table 3), which could mean that the alkali supply into the smectite started with the crystallization of the smallest nano-sized particles and could have lasted until very recently. Such a continuous process would explain the lack of radiogenic ^{40}Ar in some of the smallest nano-sized particles. In summary, partial illitization of the smectite appeared to start at

~45 Ma, during progressive burial of the host sediments when the ambient temperature was beyond 60°C. The supply of K and Rb remained limited, even if it lasted for ~12 Ma at least or even until the present time.

On the basis of the results above, alteration of the Campos bentonites involved a two-type process (smectitization followed by illitization), combined or not. Initially, pure smectite crystallized when the glass shards were altered in contact with pore fluids probably expelled from surrounding turbidites. Potassium (and Rb) supply initiated nucleation of illite layers, especially those present now in the finer <0.02 and 0.02–0.05 μm fractions, highlighted by the array joining the two finer residues of sample B1. Since deposition of the volcanic ash at 86–84 Ma, illite crystallization could have started ~40 Ma later, and ending after ~25 Ma. For some illite layers, the process could even have lasted until very recently. This crystallization with some K supply may have been induced by a changing composition of the interstitial fluids or by a changing temperature that could have been at ~25 Ma.

In summary, Rb-Sr and K-Ar isotopic results of Santonian bentonites support following evolutionary steps in the Campos Basin: a burial-induced smectitization starting in the ash beds when the volcano sediments reached a temperature of ~50–55°C probably ~44 ± 4 Ma ago, followed by a very limited illitization until 30–24 Ma, while the temperature continued to increase slightly. Illitization could have lasted longer, until 12 ± 2 Ma, fueled by a low sedimentation rate and a low geothermal gradient, and even until very recently at 0 Ma, both ages depending on the type of host bentonites. The overall occurrence of smectite confirms that burial temperature was at the lower limit of the 'illitization window,' at least in the bentonite beds, and that no significant K supply could be detected at the beginning of the alteration process. The Sr isotopic composition of the leachates is systematically above the Sr isotopic value of the seawater, during the ash deposition but also during the diagenetic episode, which suggests a 'cleaning' of layer edges from illite-smectite crystals during gentle acid leaching.

CONCLUSIONS

In the present study, X-ray determinations were combined with K-Ar and Rb-Sr analyses and electron-microscope observations of Santonian (85.8–83.5 Ma) nm-sized bentonite fractions (<0.02, 0.02–0.05 and 0.05–0.1 μm) buried to ~2800 m in the Campos Basin, offshore Rio de Janeiro State (Brazil). Unlike previous, similar mineralogical, chemical, and isotopic studies of nm-sized illite-rich mixed layers or pure illite crystals of bentonite units, the aim here was to decrypt the initial illitization stage including a limited K fixation after or during alteration of the volcanic ash into smectite, at a burial temperature always <85°C and limited interactions with pore fluids that originated in the hosting turbidites.

Based on the XRD data, the smectite crystals contain <7% illite layers. Their K-Ar data organize into three groups. One with

values from 42.6 ± 3.2 to 70.2 ± 2.1 Ma includes the size fractions with detrital illite, thus at least the K-Ar data beyond 43 Ma have no geological meaning. The second group of samples yielded younger K-Ar ages from 15.5 ± 10.7 to 46.6 ± 4.9 Ma for which the data could have some geological meaning. The last group consists of samples with varied age patterns, the smallest nano-sized fractions containing very small amounts of K and no radiogenic ^{40}Ar with analytically 0 Ma ages. The nm-sized fractions of two samples were also leached with dilute acid for Rb-Sr study with individual analyses of the untreated, leachate, and residue size fractions. The complete K-Ar and Rb-Sr database suggests that illitization probably started at 44 ± 4 Ma, smectitization being either earlier or contemporaneous.

The Rb-Sr and K-Ar isotopic data combined with the mineralogical results also provide some information about the evolution of the bentonite beds from the Campos Basin. Indeed, the smectite-rich mixed layers of sample B1 appear polluted by remnants of the volcanic ash. Local conditions in the basin could not be checked but were probably variable due to deposition of turbidites; illitization remained limited due to the slow temperature increase and probably a limited supply of alkalis. A further change occurred at an uncertain time between 24 and 30 Ma, with a likely slowing of illitization. These conditions probably changed because the fluid supply became somewhat restricted, or the fluid chemistry changed around the bentonites collected. Illite layers continued to crystallize and grow afterward, however, until the final 0 Ma age which may represent a very recent supply of K for which radioactive ^{40}K could not decay enough to be detected analytically.

REFERENCES

Altaner, S.P. & Ylagan, R.F. (1997). Comparison of structural models of mixed-layer illite/smectite and reaction mechanisms of smectite illitization. *Clays and Clay Minerals 45*, 517–533.

Altaner, S.P., Hower, J., Whitney, G., & Aronson, J.L. (1984). Model for K-bentonite formation: Evidence from zoned K-bentonites in the Disturbed Belt, Montana. *Geology 12*, 412–425.

Alves, D.B., Mizusaki, A.M.P., & Caddah L.E.G. (1993). Camadas de cinzasvulcanicas no Santoniano (Creticeo Superior) da Bacia de Campos. Simposio de Geologia do Sudeste, 3, Rio de Janeiro, SBG, Atas, 37–42.

Aronson, J.L. & Douthitt, C.B. (1986). K/Ar systematics of an acid-treated illite/smectite: Implications for evaluating age and crystal structure. *Clays and Clay Minerals 34*, 473–482.

Aronson, J.L. & Hower, J. (1976). Mechanism of burial metamorphism of argillaceous sediment: 2. Radiogenic argon evidence. *Geological Society of America Bulletin 87*, 738–744.

Bonhomme, M., Thuizat, R., Pinault, Y., Clauer, N., Wendling, R., & Winkler, R. (1975). Méthode de datation potassium-argon. Appareillage et technique. Rapport technique du Centre de Géochimie de la Surface, Université Louis Pasteur, Strasbourg, France, 53 pp.

Burst, J.F. (1959). Post diagenetic clay mineral-environmental relationships in the Gulf Coast Eocene in clays and clay minerals. *Clays and Clay Minerals 6*, 327–341.

Caddah, L.F.G., Alves, D.B., & Mizusaki, A.M.P. (1998). Turbidites associated with bentonites in the Upper-Cretaceous of the Campos Basin, offshore Brazil. *Sedimentary Geology 115*, 175–184.

Cainelli, C. & Mohriak, W.U. (1999). Some remarks on the evolution of sedimentary basins along the eastern Brazilian continental margin. *Episodes 22*, 206–216.

Calarge, L.M., Meunier, A. & Formoso M.L. (2002). A bentonite bed in the Acegua (RS, Brazil) and Melo (Uruguay) areas: a highly crystallized montmorillonite. *Journal of South American Earth Sciences 16*, 187–198.

Cardoso, R.A. & Hamza, V.M. (2014). Heat flow in the Campos sedimentary basin and thermal history of the continental margin of southeast Brazil. *ISRN Geophysics*, Hindawi Publication Corporation Article ID 384752, 19 pages.

Chang, H.K., Kowsmann, R.O., Figueiredo, A.M.F., & Bender, A.A. (1992). Tectonics and stratigraphy of the East Brazil rift system: an overview. In: Ziegler P.A. (Ed.), Geodynamics of Rifting, Volume II. Case History Studies on Rifts: North and South America and Africa. *Tectonophysics 213*, 97–138.

Clauer, N. (1982). Strontium isotopes of Tertiary phillipsites from the Southern Pacific: timing of the geochemical evolution. *Journal of Sedimentary Petrology 52*, 1003–1009.

Clauer, N. (2011). Another insight into the illitization process by K-Ar dating of micro- to nanometric illite-type particles leached with alkylammonium cations. *Clay Minerals 46*, 593–612.

Clauer, N. & Mongodin, Y. (2012). Chemical and isotopic (K-Ar) systematic of a mylonitic mica after natural and experimental interactions with varied fluids. *Chemical Geology 294-295*, 18–25.

Clauer, N., Giblin, P., & Lucas, J. (1984). Sr and Ar isotope studies of detrital smectites from the Atlantic Ocean (DSDP, Leg 43, 48 and 50). *Chemical Geology (Isotope Geosciences Section) 2*, 141–151.

Clauer, N., Chaudhuri, S., Kralik, M., & Bonnot-Courtois, C. (1993). Effects of experimental leaching on Rb-Sr and K-Ar isotopic systems and REE contents of diagenetic illite. *Chemical Geology 103*, 1–16.

Clauer, N., Środoń, J., Francù, J., & Šucha, V. (1997). K-Ar dating of illite fundamental particles separated from illite/smectite. *Clay Minerals 32*, 181–196.

Clauer, N., Rinckenbach, T., Weber, F., Sommer, F., Chaudhuri, S., & O'Neil, J.R. (1999). Diagenetic evolution of clay minerals in oil-bearing Neogene sandstones and associated shales from Mahakam Delta basin (Kalimantan, Indonesia). *American Association of Petroleum Geologists Bulletin 83*, 62–87.

Clauer, N., Liewig, N., Pierret, M.C., & Toulkeridis, T. (2003). Crystallization conditions of fundamental particles from mixed-layers illite-smectite of bentonites based on isotopic data (K-Ar, Rb-Sr & δ18O). *Clays and Clay Minerals 51*, 664–674.

Clauer, N., Rousset, D., & Środoń, J. (2004). Modeled shale and sandstone burial diagenesis based on the K-Ar systematics of illite-type fundamental particles. *Clays and Clay Minerals 52*, 576–588.

Clauer, N., O'Neil, J.R., Honnorez, J., & Buatier, M. (2011). 87Sr/86Sr and 18O/16O ratios of clay minerals from a hydrothermal mound near the Galapagos rift as records of origin, crystallization temperature and fluid composition. *Marine Geology 288*, 32–42.

Clauer, N., Williams, L., Lemarchand, D., Florian, P., & Honty, M. (2018). Illitization decrypted by B and Li isotope geochemistry of nanometer-sized illite crystals of bentonite beds from East Slovak Basin. *Chemical Geology 477*, 177–194.

Contreras, J. (2011). Seismo-stratigraphy and numerical basin modeling of the southern Brazilian continental margin (Campos, Santos and Pelotas basins). PhD thesis, University Heidelberg, Germany, 146 pp.

Dunoyer de Segonzac, G. (1970). The transformation of clay minerals during diagenesis and low-grade metamorphism: A review. *Sedimentology 15*, 281–346.

Eberl, D.D. & Środoń, J. (1988). Ostwald ripening and interparticle diffraction effects from illite crystals. *American Mineralogist 73*, 1335–1345.

Eberl, D.D., Drits, V.A., & Środoń, J. (1998). Deducing growth mechanisms for minerals from the shapes of crystals size distributions. *American Journal of Science 298*, 571–577.

Ehrenberg, S.N. & Nadeau, P.H. (1989). Formation of diagenetic illite in sandstones of the Garn Formation, Haltenbanken area, mid-Norwegian continental shelf. *Clay Minerals 24*, 233–253.

Elliott, W.C. & Aronson, J.L. (1987). Alleghanian episode of K-bentonites illitization in the southern Appalachian Basin. *Geology 15*, 735–739.

Elliott, W.C. & Haynes, J. (2002). The chemical character of fluids forming diagenetic illite in the Southern Appalachian Basin. *American Mineralogist 87*, 1519–1527.

Essene, E.J. & Peacor, D.R. (1995). Clay mineral thermometry – a critical prospective. *Clays and Clay Minerals 43*, 540–553.

Gillot, P.-Y. & Cornette, Y. (1986). The Cassignol technique for Potassium-Argon dating, precision and accuracy: Examples from the Late Pleistocene to Recent volcanics from southern Italy. *Chemical Geology (Isotope Geoscience Section) 59*, 205–222.

Hamilton, P.J., Kelley, S., & Fallick, A.E. (1989). K-Ar dating of illite in hydrocarbon reservoirs. *Clay Minerals 24*, 21–31.

Hamilton, P.J., Giles, M.R., & Ainsworth, P. (1992). K-Ar dating of illites Brent Group reservoirs: A regional perspective. In: Morton A.C, Haszeldine R.S., Giles M.R. and Brown S. (Eds). *Geology of the Brent Group*, Geological Society of London, U.K., Special Publication 61, 377–400.

Harper, C.T. (1970). Graphic solution to the problem of 40Ar loss from metamorphic minerals. *Eclogae Geologicae Helvetiae 63*, 119–140.

Hodell, D.A., Mead, G., & Mueller, P.A. (1990). Variation in the strontium isotopic composition of seawater (8 Ma to present); implications for chemical weathering rates and dissolved fluxes to the oceans. *Chemical Geology (Isotope Geosciences Section) 80*, 291–307.

Honty, M., Uhlík, P., Šucha, V., Caplovicová, M., Francù, J., Clauer, N., & Biron, A. (2004). Smectite to illite alteration in salt-bearing bentonites (The East Slovak Basin). *Clays and Clay Minerals 52*, 533–551.

Hower, J., Eslinger, E.V., Hower, M., & Perry, E.A. (1976). Mechanism of burial metamorphism of argillaceous sediments. 1. Mineralogical and chemical evidence. *Geological Society of America Bulletin 87*, 725–737.

Hunziker, J.C., Frey, M., Clauer, N., Dallmeyer, R.D., Friedrichsen, H., Flemig, W., Hochstrasser, K., Roggwiler, P., & Schwander, H. (1986). The evolution of illite to muscovite: mineralogical and isotopic data from the Glarus Alps, Switzerland. *Contributions to Mineralogy and Petrology 92*, 157–180.

Hurley, P.M., Cormier, R.F., Hower, J., Fairbairn, H.W., & Pinson, W.H. (1960). Reliability of glauconite for age measurements by K-Ar and Rb-Sr methods. *American Association of Petroleum Geologists Bulletin 44*, 1793–1808.

Inoue, A., Kohyama, N., Kitagawa, R., & Watanabe, T. (1987). Chemical and morphological evidence for the conversion of smectite to illite. *Clays and Clay Minerals 35*, 111–120.

Jackson, M.L. (1975). *Soil Chemical Analysis – Advanced Course*. Madison, Wisconsin, USA, 386 pp.

Jones, C.E. & Jenkyns, H.C. (2001). Seawater strontium isotopes, oceanic anoxic events, and seafloor hydrothermal activity in the Jurassic and Cretaceous. *American Journal of Sciences 301*, 112–149.

Kumar, N., Gamboa, L.A.P., Schreiber, B.C., & Macle, J. (1977). Geologic history and origin of the Sao Paulo Plateau (Southeastern Brazilian Margin), comparison with the Angolan Margin and early evolution of the Northern South Atlantic. *Initial Reports of Deep Sea Drilling Project, 39*, Washington D.C., pp. 927–945.

Lee, M.C., Aronson, J.L., & Savin, S.M. (1989). Timing and conditions of Permian Rotliegendes sandstone diagenesis, southern North Sea: K/Ar and oxygen isotope data. *American Association of Petroleum Geologists Bulletin 73*, 195–215.

Lee, J.Y., Marti, K., Severinghaus, J.P., Kawamura, K., Yoo, H.S., Lee, J.B., & Kim, J.S. (2006). A redetermination of the isotopic abundances of atmospheric Ar. *Geochimica et Cosmochimica Acta 70*, 4507–4512.

Lerman, A., Ray, B.M., & Clauer, N. (2007). Radioactive production and diffusional loss of radiogenic ^{40}Ar in clays in relation to its flux to the atmosphere. *Chemical Geology 243*, 205–224.

Liewig, N., Clauer, N., & Sommer, F. (1987). Rb-Sr and K-Ar dating of clay diagenesis in Jurassic sandstone oil reservoir, North Sea. *American Association of Petroleum Geologists Bulletin 71*, 1467–1474.

Ludwig, K.R. (2003). User's Manual for Isoplot/Ex Version 2.02. A geochronological Toolkit for Microsoft Excel, Berkeley Geochronology Center, Special Publication 1a, Berkeley, California, USA.

Mohriak, W.U., Mello, M.R., Karner, G.D., Dewey, J.F., & Maxwell, J.R. (1990). Structural and stratigraphic evolution of the Campos Basin, offshore Brazil. In: Tankard A.J. and Balkwill H.R. (Eds.) Extensional tectonics and stratigraphy of the North Atlantic margins. *American Association of Petroleum Geologists Memoir 46*, 577–598.

Mohriak, W.U., Rosendahl, B.R., Turner, J.P., & Valente, S.C. (2002). Crustal architecture of South Atlantic volcanic margins. In: Menzies M.A., Klemperer S.L., Ebinger C.J. and Baker J. (Eds.) Volcanic rifted margins. *Geological Society of America, Special Paper 362*, 159–202.

Nadeau, P.H., Wilson, M.J., McHardy, W.J., & Tait, J.M. (1984). Interstratified clays as fundamental particles. *Science 225*, 923–925.

Odin, G.S. and 32 collaborators (1982). Interlaboratory standards for dating purposes. In: Odin G.S. (ed.) *Numerical Dating in Stratigraphy*, J. Wiley and Sons, Chichester, UK, pp. 123–149.

Odin, G.S. & Bonhomme, M.G. (1982). Argon behavior in clays and glauconies during preheationg experiments. In: Odin G.S. (Ed.), *Numerical Dating in Stratigraphy*, J. Wiley and Sons, Chichester, UK, pp. 333–344.

Odin, G.S., Velde, B., & Bonhomme, M. (1977). Radiogenic argon retention in glauconites as a function of mineral recrystallization. *Earth and Planetary Science Letters 37*, 154–158.

Ojeda, H.A. (1982). Structural framework, stratigraphy and evolution of Brazilian marginal basins. *American Association of Petroleum Geologists Bulletin 66*, 732–749.

Perry, E.A. Jr. (1974). Diagenesis and the K-Ar dating of shales and clay minerals. *Geological Society of America Bulletin 85*, 827–830.

Pevear, D.R. (1992). Illite age analysis, a new tool for basin thermal history analysis. In: Kharaka Y.K and Maest A.S. (eds.), Proceedings of the 7th International Symposium on Water-Rock Interaction, Balkema, Rotterdam, Netherlands 1251–1254.

Pollastro, R.M. (1993). Considerations and applications of the illite/smectite geothermometer in hydrocarbon-bearing rocks of Miocene to Mississippian age. *Clays and Clay Minerals 41*, 119–133.

Powers, M.C. (1959). Adjustment of clays to chemical change and the concept of the equivalence level. *Clays and Clay Minerals 6*, 309–326.

Renac, C. & Meunier A. (1995). Reconstruction of paleothermal conditions in a passive margin using illite–smectite mixed-layer series (BA1 scientific deep drill-hole, Ardèche, France). *Clay Minerals 30*, 107–118.

Reuter, A. (1987). Implications of K-Ar ages of whole-rocks and grain-size fractions of metapelites and intercalated metatuffs within an anchizonal terrane. *Contributions to Mineralogy and Petrology 97*, 105–115.

Schaltegger, U., Stille, P., Rais, N., Piqué, A., & Clauer, N. (1994). Nd and Sr isotopic dating of diagenesis and low-grade metamorphism of argillaceous sediments. *Geochimica et Cosmochimica Acta 58*, 1471–1481.

Środoń, J. (1980). Precise identification of illite/smectite interstratification by X-ray powder diffraction. *Clay Minerals 28*, 401–411.

Środoń, J. & Eberl, D.D. (1984). Illite. In: Bailey S.W. (Ed.) *Micas*. Reviews in Mineralogy 13, Mineralogical Society of America, Washington, DC, 584 pp.

Środoń, J., Elsass, F., McHardy, W.J., & Morgan, D.J. (1992). Chemistry of illite/smectite inferred from TEM measurements of fundamental particles. *Clay Minerals 27*, 137–158.

Środoń, J., Clauer, N., & Eberl, D.D. (2002). Interpretation of K-Ar dates of illitic clays from sedimentary rocks aided by modelling. *American Mineralogist 87*, 1528–1535.

Środoń, J., Clauer, N., Banas, M., & Wojtowicz, A. (2006). K-Ar evidence for a Mesozoic thermal event superimposed on burial diagenesis of the Upper Silesia Coal Basin. *Clay Minerals 41*, 669–690.

Środoń, J., Zeelmaekers, E., & Derkowski, A. (2009a). The charge of component layers of illite-smectite in bentonites and the nature of end-member illite. *Clays and Clay Minerals 57*, 649–671.

Środoń, J., Clauer, N., Huff, W.D., Dudek, T., & Banas M. (2009b). K-Ar dating of Ordovician K-bentonites from the Baltic Basin and the Baltic Shield: implications for the role of temperature and time in the illitization of smectite. *Clay Minerals 44*, 361–387.

Środoń, J., Kuzmenkova, O., Stanek, J.J., Petit, S., Beaufort, D., Gilg, H.A., Liivamägi, S., Goryl, M., Marynowski, L., & Szczerba, M. (2019). Hydrothermal alteration of the Ediacaran Volyn-Brest volcanics on the western margin of the East European Craton. *Precambrian Research 325*, 217–235.

Steiger, R. & Jäger, E. (1977). Subcommission on Geochronology: Convention on the use of decay constants in geo-cosmochronology. *Earth and Planetary Science Letters 36*, 359–362.

Šucha, V., Kraus, I., Gerthofferová, H., Peteš, J., & Sereková, M. (1993). Smectite to illite conversion in bentonites and shales of the East Slovak Basin. *Clay Minerals 28*, 243–253.

Szczerba, M., Derkowski, A., Kalinichev, A.G., & Środoń, J. (2015). Molecular modeling of the effects of ^{40}Ar recoil in illite particles on their K–Ar isotope dating. *Geochimica et Cosmochimica Acta 159*, 162–176.

Thompson, G.R. & Hower, J. (1973). An explanation for low radiometric ages from glauconite. *Geochimica and Cosmochimica Acta 37*, 1473–1491.

Turekian, K.K. & Wedepohl, K.H. (1961). Distribution of the elements in some major units of the Earth's crust. *Geological Society of America Bulletin 72*, 175–192.

Velde, B. (1985). *Clay Minerals: A Physico-chemical Explanation of their Occurrence*. Developmentss in Sedimentology 40, Elsevier, Amsterdam, 426 pp.

Velde, B. & Vasseur, G. (1992). Estimation of the diagenetic smectite to illite transformation in time-temperature space. *American Mineralogist 77*, 967—976.

Viana, A.R., Faugères, J.C., Kowsmann, R.O., Lima, J.A.M., Caddah, L.F.G., & Rizzo, J.G. (1998). Hydrology, morphology and

sedimentology of the Campos continental margin, offshore Brazil. *Sedimentary Geology 115*, 133–157.

Weaver, C.E. (1957). The clay petrology of sediments. *Clays and Clay Minerals 6*, 154–187.

Zimmermann, J.L. & Odin, G.S. (1982). Kinetics of the release of argon and fluids from glauconies. In: Odin G.S. (Ed.) *Numerical Dating in Stratigraphy*. J. Wiley Publisher, Chichester, UK, pp. 345–362.